The transfer of a mitochondrial selfish element to the nuclear genome and its consequences

Julien Y. Dutheil[1,2,3,*], Karin Münch[2], Klaas Schotanus[2,4], Eva H. Stukenbrock[1,2,4], Regine Kahmann[2]

1. Max Planck Institute for Evolutionary Biology
August-Thienemann-Str. 2
24306 Plön, Germany

2. Max Planck Institute for Terrestrial Microbiology
Karl-von-Frisch-Str. 10
35043 Marburg, Germany

3. Institute of Evolutionary Sciences
CNRS - University of Montpellier – IRD - EPHE
Place Eugène Bataillon, 34095 Montpellier, France.

4. Christian Albrechts University of Kiel
24118 Kiel, Germany

Correspondence:
* Julien Y. Dutheil, dutheil@evolbio.mpg.de

Running head: Recent transfer of a mitochondrial homing endonuclease

Keywords: homing endonuclease, mitochondrion, intron, gene birth, gene transfer

Abstract

Homing endonucleases (HE) are enzymes capable of excising their encoding gene and inserting it in a highly specific target sequence. As such, they act both as intronic sequences (type-I introns) and selfish invasive elements. HEs are present in all three kingdoms of life and viruses; in eukaryotes, they are mostly found in the genomes of mitochondria and chloroplasts, as well as nuclear ribosomal RNAs. We here report the case of a HE that integrated into a telomeric region of the fungal maize pathogen *Ustilago maydis*. We show that the gene has a mitochondrial origin, but its original copy is absent from the *U. maydis* mitochondrial genome, suggesting a subsequent loss or a horizontal transfer. The telomeric HE underwent mutations in its active site and acquired a new start codon, but we did not detect significant transcription of the newly created open reading frame. The insertion site is located in a putative RecQ helicase gene, truncating the C-terminal domain of the protein. The truncated helicase is expressed during infection of the host, together with other homologous telomeric helicases. This unusual homing event represents a singular evolutionary time point: the creation of two new genes whose fate is not yet written. The HE gene lost its homing activity and can potentially acquire a new function, while its insertion created a truncated version of an existing gene, possibly altering its original function.

Introduction

The elucidation of the mechanisms at the origin of genetic variation is a longstanding goal of molecular evolutionary biology. Mutation accumulation experiments - together with comparative analysis of sequence data - are instrumental in studying the processes shaping genetic diversity at the molecular level (Kondrashov and Kondrashov 2010; Eyre-Walker and Keightley 2007). They revealed that the spectrum of mutations ranges from single nucleotide substitutions to large scale chromosomal rearrangements, and encompasses insertions, deletions, inversions, and duplication of genetic material of variable length (Lynch et al. 2008). Mutation events may result from intrinsic factors such as replication errors and repair of DNA damage. In some cases, however, mutations can be caused or favored by extrinsic factors, such as mutagenic environmental conditions or parasitic genome entities like viruses or selfish mobile elements. Such particular sequences, able to replicate and invade the host genome, may have multiple effects including inserting long stretches of DNA that do not encode any organismic function, but also disrupting, copying and moving parts of the genome sequence. These selfish element-mediated mutations can significantly contribute to the evolution of their host: first, the invasion of these elements creates “junk” DNA that can significantly increase the genome size (Lynch 2007), and some of this material can be ultimately domesticated and acquire a new function, beneficial to the host (Kaessmann 2010; Volff 2006). Second, the genome dynamics resulting from the activity of these elements can generate novelty by gene duplication (Ohta 2000; Dutheil et al. 2016) or serve as a mechanism of parasexuality and compensate for the reduced diversity in the absence of sexual reproduction (Dong et al. 2015; Möller and Stukenbrock 2017). Finally, mechanisms that evolved to control these elements (such as repeat-induced point mutations in fungi (Gladyshev 2017)) may also incidentally affect genetic diversity (Grandaubert et al. 2014).

Selfish elements whose impact on genome evolution is less well documented are the homing endonuclease genes (HEG), encoding a protein able to recognize a particular genomic DNA sequence and cut it (homing endonuclease, HE). The resulting double-strand break is subsequently repaired by homologous recombination using the HEG itself as a template, resulting in its insertion in the target location (Stoddard 2005). As the recognized sequence is highly specific, the insertion typically happens at a homologous position. In this process, a *heg*$^+$ element containing the endonuclease gene converts a *heg*$^-$ allele (devoid of HEG but harbouring the recognition sequence) to *heg*$^+$, a mobility mechanism referred to as *homing* (Dujon et al. 1989). After the insertion, the host cell is homozygous *heg*$^+$, and the HEG segregates at a higher frequency than the Mendelian rate (Goddard and Burt 1999). The open reading frame of the HEG is included in a sequence capable of self-splicing, either at the RNA or protein level, avoiding disruption of functionality when inserted in a protein-coding gene. This mechanism results in the so-called group-I introns or inteins, respectively (Chevalier and Stoddard 2001; Stoddard 2005). The dynamic of HEGs has been well described, and involves three stages: (i) conversion from *heg*$^-$ to *heg*$^+$ by homing activity, (ii) degeneration of the HEG leading to the loss of homing activity, but still protecting against a new insertion because the target is altered by the insertion event and (iii) loss of the HEG leading to the restoration of the *heg*$^-$ allele (Gogarten and Hilario 2006; Barzel et al. 2011). This cycle leads to recurrent gains and losses of HEG at a given genomic position, and ultimately to the loss of the HEG at the population level unless new genes invade from other locations or by horizontal gene transfer (Gogarten and Hilario 2006).

HEGs are found in all kingdoms of life as well as in the genomes of organelles, mitochondria and chloroplasts (Stoddard 2005; Lambowitz and Belfort 1993; Belfort and Roberts 1997). In several fungi, HEGs are residents of mitochondria. Here, we study the molecular evolution of a HEG from the fungus *Ustilago maydis*, which serves as a model for the elucidation of (1) fundamental biological processes like cell polarity, morphogenesis, organellar targeting, and (2) the mechanisms allowing biotrophic fungi to colonize plants and cause disease (Steinberg and

Perez-Martin 2008; Djamei and Kahmann 2012; Vollmeister et al. 2012; Ast et al. 2013). *U. maydis* is the most well-studied representative of smut fungi, a large group of plant pathogens, because of the ease by which it can be manipulated both genetically and through reverse genetics approaches (Vollmeister et al. 2012). Besides, its compact, fully annotated genome comprises only 20.5 Mb and is mostly devoid of repetitive DNA (Kämper et al. 2006). The genome sequences of several related species, *Sporisorium reilianum*, *S. scitamineum* and *Ustilago hordei* causing head smut in corn, smut whip in sugarcane and covered smut in barley, respectively, provide a powerful resource for comparative studies (Schirawski et al. 2010; Laurie et al. 2012; Dutheil et al. 2016). We report here the case of a gene from *U. maydis,* which we demonstrate to be a former mitochondrial HEG recently integrated into the nuclear genome. The integration of the gene has truncated the gene containing the insertion, followed by inactivation of the endonuclease active site, which generated a new open reading frame that contains the DNA-binding domain of the HEG (Derbyshire et al. 1997).

Results

We report the analysis of the nuclear gene *UMAG_11064* from the smut fungus *U. maydis*, which was identified as an outlier in a whole-genome analysis of codon usage. We first provide evidence that the gene is a former HEG and then reconstruct the molecular events that led to its insertion in the nuclear genome using comparative sequence analysis. Finally, we assess the phenotypic impact of the insertion event.

The *UMAG_11064* nuclear gene has a mitochondrial codon usage.

We studied the synonymous codon usage in protein-coding genes of the smut fungus *U. maydis*, using within-group correspondence analysis. As opposed to other methods, within-group correspondence analysis allows to compare codon usage while adequately taking into account confounding factors such as variation in amino-acid usage (Perrière and Thioulouse 2002). We report a distinct synonymous codon usage for nuclear genes and mitochondrial genes (Figure 1A), with the notable exception of the nuclear gene *UMAG_11064,* which displays a typical mitochondrial codon usage. The *UMAG_11064* gene is located in the telomeric region of chromosome 9, with no further downstream annotated gene (Figure 1B). It displays a low GC content of 30%, which contrasts with the GC content of the flanking regions (50%) and the rather homogeneous composition of the genome sequence of *U. maydis* as a whole. It is, however, in the compositional range of the mitochondrial genome (Figure 1B). Altogether, the synonymous codon usage and GC content of *UMAG_11064* suggest a mitochondrial origin.

In order to confirm the chromosomal location of *UMAG_11064*, we amplified and sequenced three regions encompassing the gene using primers within the *UMAG_11064* gene and primers in adjacent chromosomal genes upstream and downstream of *UMAG_11064* (Figure S1). The sequences of the amplified segments were in full agreement with the genome sequence of *U. maydis* (Kämper et al. 2006), thereby ruling out possible assembly artefacts in this region. Surprisingly, the sequence of *UMAG_11064* has no match in the mitochondrial genome of *U. maydis* (GenBank entry NC_008368.1), which suggests that *UMAG_11064* is an authentic nuclear gene. As both the GC content and synonymous codon usage of *UMAG_11064* are indistinguishable from the ones of mitochondrial genes and have not moved toward the nuclear equilibrium, the transfer of the gene to its nuclear position must have occurred recently.

The *UMAG_11064* gene contains parts of a former GIY-YIG homing endonuclease

To gain insight into the nature of the *UMAG_11064* gene, its predicted nucleotide sequence was searched against the NCBI non-redundant nucleotide sequence database. High similarity matches were found in the mitochondrial genome of three other smut fungi (Supplementary Table S1): *S. reilianum* (87% identity), *S. scitamineum* (79%), and *U. bromivora*

(76%). Two other very similar sequences were found in the mitochondrial genome of two other smut fungi, *Tilletia indica* and *Tilletia walkeri*, as well as in mitochondrial genomes from other basidiomycetes (e.g. *Laccaria bicolor*) and ascomycetes (e.g. *Leptosphaeria maculans*, see Supplementary Table S1). The protein sequence of *UMAG_11064* shows high similarity with fungal HEGs, in particular of the so-called GIY-YIG family (Supplementary Table S2) (Stoddard 2005). The closest fully annotated protein sequence matching *UMAG_11064* corresponds to the GIY-YIG HEG located in intron 1 of the *cox1* gene of *Agaricus bisporus* (I-AbiIII-P). The amino-acid sequence of UMAG_11064 matches the N-terminal part of this protein containing the DNA-binding domain of the HE (Derbyshire et al. 1997). As the GC profile of *UMAG_11064* suggests that the upstream region also has a mitochondrial origin (Figure 1B), we performed a codon alignment of the 5' region with the full intron sequence of *A. bisporus*, *T. indica* and *T. walkeri* as well as the sequence of I-AbIII-P in order to search for putative traces of the activity domain of the HE (Figure 2). We used the Macse software (Ranwez et al. 2011) to infer codon alignment in the presence of frameshifts. We found that the intergenic region between *UMAG_11065* and *UMAG_11064* displays homology to the activity domain of other GIY-YIG HE, and contains remnants of the former active site of the type GVY-YIG (Figure 2). Compared to I-AbiIII-P and homologous sequences in *Tilletia*, however, a frameshift mutation has occurred in the active site (a 7 bp deletion). The predicted gene model for *UMAG_11064,* therefore, starts at a conserved methionine position, 14 amino-acids downstream of the former active site (Figure 2). Altogether, these results suggest that *UMAG_11064* is a former HE which inserted into the nuclear genome, was then inactivated by a deletion in its active site and acquired a new start codon.

The *UMAG_11064* gene is similar to an intronic mitochondrial sequence of *S. reilianum*

The closest homologous sequence of *UMAG_11064* was found in the first intron of the *cox1* gene of the smut fungus *S. reilianum* while this sequence was absent in the mitochondrial genome of *U. maydis*. The *cox1* genes of *S. reilianum* and *U. maydis* both have eight introns, of which only seven are homologous in position and sequence (Figure 3). *S. reilianum* has one extra intron in position 1, while *U. maydis* has one extra intron in position 6. In *U. maydis* all introns but the sixth one are reported to be of type I, *i.e.* contain a HEG which is responsible for their correct excision. A blast search of this intron's sequence, however, revealed similarity with a homing endonuclease of type LAGLIDADG (Supplementary Table S4). In *S. reilianum*, intron 1 (the putative precursor of *UMAG_11064)* and intron 2 are not annotated as containing a HEG. Blast searches of the corresponding sequences, however, provided evidence for homology with a GIY-YIG HE (Supplementary Table S5) and a LAGLIDADG HE, respectively (Supplementary Table S6).

Furthermore, intron 1 in *S. reilianum* was not detected in *U. maydis*. A closer inspection showed that the ORF could be aligned with related HEs (Figure 2). This alignment revealed an insertion of four amino-acids, a deletion of the first glycine residue in the active site plus several frameshifts at the beginning of the gene, which suggests that this gene has been altered and might not encode a functional HE any longer.

UMAG_11064 inserted into a gene encoding a RecQ helicase

In order to study the effect of the HEG insertion in the nuclear genome, we looked at the genomic environment of the *UMAG_11064* gene. Downstream of *UMAG_11064* are telomeric repeats, while the next upstream gene, *UMAG_11065*, is uncharacterized. A similarity search for *UMAG_11065* detected 13 homologous sequences in the *U. maydis* genome (including one, *UMAG_12076*, on an unmapped contig), but only low-similarity matches in other sequenced smut fungi (see Methods). The closest non-smut related sequence comes from a gene from *Fusarium oxysporum*. We inferred the evolutionary relationships between the 14 genes by reconstructing a maximum likelihood phylogenetic tree, and found that the *UMAG_11065* gene is closely related to

UMAG_04486, located on chromosome 14 (Figure 4 and Table 1). The *UMAG_04486* gene, however, is predicted to be almost six times as long as *UMAG_11065*, suggesting that the latter was truncated because of the *UMAG_11064* insertion. A search for similar sequences of *UMAG_11065* and its relatives in public databases revealed homology with so-called RecQ helicases (Supplementary Table S3), enzymes known to be involved in DNA repair and telomere expansion (Singh et al. 2012). While this function is only predicted by homology, we note that all 12 chromosomal *recQ* related genes are located very close to telomeres in *U. maydis* (Table 1), suggesting a role of these gene in telomere maintenance (Sánchez-Alonso and Guzmán 1998). Interestingly, this gene family also contains the gene *UMAG_03394*, which is located four genes upstream of *UMAG_11065*. Chromosome 9 appears to be the only chromosome with two helicase genes on the same chromosome end (Table 1).

U. maydis populations shows structural polymorphism in the telomeric region of chromosome 9

Because the *UMAG_11064* gene still displays a strong signature of its mitochondrial origin (codon usage and GC content), its transfer most likely occurred recently. In order to provide a timeframe for the insertion event, we examined the structure of the genomic region of the insertion in other *U. maydis* and *S. reilianum* isolates, as well as the structure of the *cox1* exons 1, 2 and 7. The regions that could be amplified and their corresponding sizes are listed in Table 2. The *UMAG_11064* gene is present in the FB1-derived strain SG200, as well as the Holliday strains 518 and 521, but is absent in nuclear as well mitochondrial genome sequences of a recent *U. maydis* isolate from the US, strain 10-1, as well as from 5 Mexican isolates (I2, O2, P2, S5 and T6, Figure S2A). The *UMAG_11072* gene, however, which is located further away from the telomere on the same chromosome arm, could be amplified in all strains (Figure S2B). All *U. maydis* strains possess intron 6 in the mitochondrial *cox1* gene, which is absent in *S. reilianum*, while the three *S.*

reilianum strains tested carry intron 1, that is absent in all *U. maydis* strains (Figure S2C-D). These results suggest that the *UMAG_11064* gene inserted in an ancestor of the two strains 518 and 521, after the divergence from other *U. maydis* strains, an event that occurred very recently. Moreover, the most direct descendant of the progenitor of the HEs, *i.e.* intron 1 in the *cox1* gene, could not be found in any of the sequenced mitochondrial genomes of *U. maydis* strains, while it is present in the three sequenced *S. reilianum* strains (Figure S2).

Functional characterization

To shed light on the functional implication of the translocation of the HEG and subsequent mutations we (i) assessed the expression profile of these genes and (ii) generated a deletion strain and phenotyped it. For the expression analysis we relied on a previously published RNASeq data set (Lanver et al. 2018), from which we extracted the expression profiles of genes in the telomeric region of chromosome 9 (Figure 5A). While the expression of *UMAG_11064* remained close to zero in the three replicates, expression of *UMAG_11065* increased during plant infection. The telomeric region was highly heterogeneous in terms of expression profile: while *UMAG_11066* and *UMAG_03393* did not show any significant level of expression, *UMAG_03392* was down-regulated starting at twelve hours post-infection, while *UMAG_03394*, another RecQ-encoding gene homologous to *UMAG_11065,* displayed constitutively high levels of expression (Figure 5A). All homologs of *UMAG_11065* show a significantly higher expression during infection (Tukey's posthoc test, false discovery rate of 5%, Figure 5B). The comparison of expression profiles revealed two main classes of genes (Figure 5C): highly expressed genes (upper group), and moderately expressed genes (lower group), to which *UMAG_11065* belongs. We further note that the differences in expression profiles do not mirror the protein sequence similarity of the genes (Mantel permutation test, p-value = 0.566).

To assess the function *UMAG_11064* and *UMAG_11065* were simultaneously deleted in SG200, a solopathogenic haploid strain that can cause disease without a mating partner (Kämper et al. 2006) using a single-step gene replacement method (Kämper 2004). Gene deletion was verified by Southern analysis (Figure S3). Virulence assays, conducted in triplicate revealed no statistically different symptoms of SG200Δ11065Δ11064 compared to SG200 in infected maize plants (Figure 6A, Chi-square test, p-value = 0.453). Since RecQ helicases contribute to dealing with replication stress (Kojic and Holloman 2012) we also determined the sensitivity of the mutant to various stressors including UV, hydroxyurea and Congo Red. (Figure 6B). We report that the deletion strain shows increased sensitivity to cell wall stress induced by Congo Red and increased resistance to UV stress. Since *UMAG_11064* does not show any detectable level of expression, we hypothesize that the deletion of *UMAG_11065* is responsible for this phenotype.

Discussion

The codon usage and GC content of the *UMAG_11064* gene, as well as its similarity to known mitochondrial HEGs, points at a recent transfer into the nuclear genome of *U. maydis*. Moreover, the precursor of this gene is absent from the mitochondrial genome of this species. To explain this pattern, we propose a scenario involving a transfer of the gene to the nuclear genome followed by a loss of the mitochondrial copy (Figure 7). We hypothesize that the mitochondrial HEG was present in the *U. maydis* ancestor. The evolutionary scenario involves two events: the insertion of the HEG into the nuclear genome, on the one hand, creating a HEG^+ genotype at the nuclear locus (designated $[HEG^+]_{nuc}$), and the loss of the mitochondrial copy, creating a HEG^- genotype at the mitochondrial locus (designated $[HEG^-]_{mit}$). These two events might have happened independently, but the former cannot have happened after the fixation of the $[HEG^-]_{mit}$ genotype in the population. The $[HEG^+]_{nuc}$ / $[HEG^-]_{mit}$ genotype could be generated by a cross between two individuals, one $[HEG^+]_{nuc}$ and the other $[HEG^-]_{mit}$, given that mitochondria are uniparentally inherited in *U. maydis* (Basse 2010). The segregation of the $[HEG^+]_{nuc}$ and $[HEG^-]_{mit}$ variants could be either neutral, and therefore driven by genetic drift, or enhanced by selection if such variants conferred an advantage to their carrier. An intriguing alternative scenario is that the mitochondrial

HEG was not ancestral to *U. maydis*, but was horizontally transferred from *S. reilianum* (or a related species). In support of this hypothesis is the high similarity of the *UMAG_11064* gene to the *S. reilianum* mitochondrial HEG (Figure 2), which contrasts with the relatively high nucleotide divergence between the two species, which diverged around 20 My ago (Schweizer et al. 2018). Besides, it is worth noting that *U. maydis* and *S. reilianum* share the same host, and that hybridization between smut species has been reported (Fischer 1957; Boidin 1986).

HEGs are found in eukaryotic nuclei but are usually restricted to small and large ribosomal RNA subunit genes (Lambowitz and Belfort 1993; Dunin-Horkawicz et al. 2006). While transfer of DNA segments and functional genes from organellar genomes to the nucleus is well documented (Sun and Callis 1993; Thorsness and Weber 1996; Lloyd and Timmis 2011; Fuentes et al. 2012), established examples of HEG insertions at other genomic locations than rRNA genes is very scarce. Louis and Haber (Louis and Haber 1991) reported such a transfer into a telomeric region of *Saccharomyces cerevisiae*. The authors argue that signatures of such insertion could be found because (1) it had no deleterious effect and (2) the occurrence of heterologous recombination between telomeres favours the maintenance of elements, which would otherwise be lost. Contrasting with this result, the insertion of the GIY-YIG HEG that inserted into the ancestor of the *UMAG_11065* gene potentially had non-neutral effects, resulting in an expressed truncated protein. The sequence of *UMAG_11064* suggests a recent transfer into the nuclear genome, but finding several mutations within the active site, the encoded protein is unlikely to be functional. As no significant level of expression was measured for this gene, this newly acquired gene is most likely undergoing pseudogenisation. However, as this mitochondrial HEG inserted into a nuclear *U. maydis* gene, it might have had phenotypic consequences not directly due to the HEG gene itself. The *UMAG_11065* gene appeared to have been truncated by the HEG insertion, which removed the C-terminal part of the encoded protein, and the truncated *UMAG_11065* is expressed during infection. While we were unable to detect a contribution to virulence, our results point at a putative role of the truncated RecQ helicase into stress tolerance, as it increases both resistance to UV radiation and susceptibility to cell wall stress. We hypothesise that the first effect is possibly due to the truncated UMAG_11065 protein interfering with telomere maintenance, making the cell more susceptible to UV damage. How the truncated UMAG_11065 RecQ helicase could improve coping with cell wall stress, however, remains to be investigated, as well as the potential fitness benefit or cost of these phenotypes.

Conclusions

In this study, we report instances of two stages of the life cycle of HEGs. Intron 1 of the mitochondrial *cox1* gene of *S. reilianum* was shown to contain a degenerated GIY-YIG HEG, while the homologous position in the *U. maydis* gene displays no intron. Besides, in the telomeric region of chromosome 9 of the nuclear genome of *U. maydis*, we found evidence of a recent migration of a very similar GIY-YIG HEG. This very rare event could be uncovered thanks to its recent occurrence and the singularly homogeneous composition of the *U. maydis* nuclear genome. It likely represents a snapshot of evolution, when a mutational event occurred, but selection did not have time yet to act. The future of this insertion remains, therefore, to be written. Its absence in any field isolates of *U. maydis* sequenced so far suggests that either the mutation was lost in natural populations, or that it occurred in the lab after the selection of the original Holliday strains. These results demonstrate that HEGs, like other mobile elements, may represent a so far understudied source of genetic diversity.

Material and Methods

Analysis of codon usage and GC content

Ustilago maydis gene models (genome version 2.0) were retrieved from the MIPS database (Mewes et al. 2011). Mitochondrial genes were extracted from the *U. maydis* full mitochondrial genome (Genbank accession number: NC_008368.1). Within-group correspondence analysis of synonymous codon usage was performed using the ade4 package for R, following the procedure described in (Charif et al. 2005). The proportion of G and C nucleotides was computed along with the first 10 kb of *U. maydis* chromosome 9, using 300 bp windows slid by 1 bp. The corresponding R code is available as Supplementary File S1.

Strains, growth conditions and virulence assays

The *Escherichia coli* strains DH5α (Bethesda Research Laboratories) and TOP10 (Life Technologies, Carlsbad, CA, USA) were used for the cloning and amplification of plasmids. *U. maydis* strains 518 and 521 are the parents of FB1 and FB2 (Banuett and Herskowitz 1989). SG200 is a hapoid solopathogenic strain derived from FB1 (Kämper et al. 2006). 10-1 is an uncharacterized haploid *U. maydis* strain isolated in the US and kindly provided by G. May. I2, O2, P2, S5, and T6 are haploid *U. maydis* strains collected in different parts of Mexico (Valverde et al. 2000). The haploid *S. reilianum* strains SRZ1 and SRZ2 as well as the solopathogenic strain JS161 derived from SRZ1 have been described (Schirawski et al. 2010). Deletion mutants were generated by gene replacement using a PCR-based approach and verified by Southern analysis (Kämper 2004).

pRS426Δum11064+11065 is a pRS426-derived plasmid containing the *UMAG_11064*/ *UMAG_11065* double deletion construct which consists of a hygromycin resistance cassette flanked by the left border of the *UMAG_11064* and right border of the *UMAG_11065* gene. The left border of *UMAG_11064* and the right border of *UMAG_11065* were PCR amplified from SG200 gDNA with primers um11064_lb_fw/um11064_lb_rv and um11065_rb_fw/um11065_rb_rv (Supplementary Table S7). The hygromycin resistance cassette was obtained from SfiI digested pHwtFRT (Khrunyk et al. 2010). The pRS426 EcoRI/XhoI backbone, both borders and the resistance cassette were assembled using yeast drag and drop cloning (Christianson et al. 1992). The fragment containing the deletion cassette was amplified from this plasmid using primers um11064_lb_fw and um11065_rb_rv, transformed into SG200 and transformants carrying a deletion of *UMAG_11064* and *UMAG_11065* were identified by southern analysis (Figure S3).

U. maydis strains were grown at 28°C in liquid YEPSL medium (0.4% yeast extract, 0.4% peptone, 2% sucrose) or on PD solid medium (2.4% Potato Dextrose broth, 2% agar). Stress assays were performed as described in (Krombach et al. 2018). Transformation and selection of *U. maydis* transformants followed published procedures (Kämper et al. 2006). To assess virulence, seven day old maize seedlings of the maize variety Early Golden Bantam (Urban Farmer, Westfield, Indiana, USA) were syringe-infected. At least three independent infections were carried out and disease symptoms were scored according to Kämper et al. (Kämper et al. 2006). Consistence of replicates was tested using a chi-squared test and p-values were computed using 1,000,000 permutations. As no significant difference between replicates was observed (p-value = 0.347 for the wildtype and p-value = 0.829 for the deletion strain), observation were pooled between all replicates for each strain before being compared.

Blast searches and gene alignment

We performed BlastN and BlastP (Altschul et al. 1990) searches using the (translated) sequence of *UMAG_11064* as a query using NCBI online blast tools. The non-redundant nucleotide and protein sequence databases were selected for BlastN and BlastP, respectively. Results were further processed with scripts using the NCBIXML module from BioPython modules (Cock et al. 2009). The Macse codon aligner (Ranwez et al. 2011) was used in order to infer the position of putative frameshifts in the upstream region of *UMAG_11064*. The alignment was depicted using the Boxshade software and was further manually annotated. The sequences of *U. maydis cox1* intron 6, as well as *S. reilianum cox1* introns 1 and 2 were used as query and searched against the protein non redundant database using NCBI BlastX, excluding environmental samples and model sequences. The *cox1* genes from *U. maydis* and *S. reilianum* were aligned and pairwise similarity was computed in non-overlapping 100 bp windows (Supplementary File S1). The gene structure, synteny and local pairwise similarity was depicted using the genoPlotR package for R (Guy et al. 2010).

Amplification of the *UMAG_11064* regions in several *U. maydis* strains

Amplification of DNA fragments via polymerase chain reaction (PCR) was done using the Phusion High Fidelity DNA_Polymerase (Thermo Fisher Scientific, Waltham, USA). The PCR reactions were set up in a 20 µl reaction volume using DNA templates indicated in the respective experiments and buffer recommended by the manufacturer containing a final concentration of 3% DMSO. The PCR programs used are represented by the following scheme: Initial denaturation – [denaturation – annealing – elongation] x number cycles – final elongation. *UMAG_11072* was amplified with primers um11072_ORF_fw x um11072_ORF_rv using 98 °C/3 m - [98 °C/10 s – 65 °C/30 s - 72 °C/45 s] x 30 cycles - 72 °C/10 m. *UMAG_11064* was amplified with primers um11064_ORF_fw x um11064_ORF_rv using 98 °C/3 m - [98 °C/10 s – 65 °C/30 s - 72 °C/45 s] x 30 cycles - 72 °C/10 m. The *cox1* exons 1+2 were amplified with primers cox1_ex1_rv x cox1_ex2_fw using 98 °C/3 m - [98 °C/10 s – 63 °C/30 s - 72 °C/90 s] x 33 cycles - 72 °C/10 m. cox1 exon 7 was amplified with primers cox1_ex7_fw X cox1_ex7_rv using 98 °C/3 m - [98 °C/10 s – 67 °C/30 s - 72 °C/60 s] x 30 cycles - 72 °C/10 m. Parts of the genomic region containing *UMAG_11064*, *UMAG_11065* and *UMAG_11066* were amplified with primer pairs um11064_fw1 x um11064_rv1, um11064_fw1 x um11064_rv2; and um11064_ fw2 x um11064_rv2 using 98 °C/3 m - [98 °C/10 s – 65 °C/30 s - 72 °C/150 s] x 32 cycles - 72 °C/10 m. The list of all primer sequences is provided in Supplementary Table S7. PCR results are shown in Figures S1 and S2.

History of the *UMAG_11065* family

The sequence of the *UMAG_11065* protein was used as a query for a search against several smut fungi (*U. maydis*, *U. hordei*, *S. reilianum*, *S. scitamineum*, *Melanopsichum pennsylvanicum*, *Pseudozyma flocculosa*), complete proteome using BlastP (Altschul et al. 1990).

The search finds 17 hits within the *U. maydis* genome with an E-value below 0.0001, as well as two genes in *Sporisorium scitamineum* (*SPSC_04622* and *SPSC_05783*) and two genes in *Pseudozyma flocculosa* (*PFL1_06135* and *PFL1_02192*). Using NCBI BlastP, we found several sequences from *Fusarium oxyparum* with high similarity. We selected the sequence *FOXG_04692* as a representative and added it to the data set. The Guidance web server with the GUIDANCE2 algorithm was then used to align the protein sequences and assess the quality of the resulting alignment. Default options from the server were kept, selecting the MAFFT aligner (Katoh et al. 2002). Several sequences appeared to be of shallow alignment quality and were discarded. The remaining sequences were realigned using the same protocol. Four iterations were performed until the final alignment had a quality good enough for phylogenetic inference. The final alignment contained 14 sequences and had a global score of 0.79. These 14 alignable sequences contained 13 *U. maydis* sequences (including *UMAG_11065*), and the *F. oxysporum* gene, other sequences from smut genomes were too divergent to be unambiguously aligned. Using Guidance, we further masked columns in the alignment with a score below 0.93 (a maximum of one position out of 14 in the column was allowed to be uncertain).

A phylogenetic analysis was conducted using the program Seaview 4 (Gouy et al. 2010). First, a site selection was performed in order to filter regions with too many gaps, leaving 506 sites. Second, a phylogenetic tree was built using PhyML within Seaview (Guindon et al. 2010) (Le and Gascuel protein substitution model (Le and Gascuel 2008) with a four-classes discretized gamma distribution of rates, the best tree of Nearest Neigbour Interchange (NNI) and Subtree Pruning and Regrafting (SPR) topological searches was kept). Support values were computed using the approximate likelihood ratio test (aLRT) method (Anisimova and Gascuel 2006). The resulting tree was rooted using the midpoint rooting method in Seaview.

Gene expression

RNASeq normalized expression counts for the *UMAG_11064* and *UMAG_11065*, as well as of neighbouring genes and paralogs elsewhere in the genome, were extracted from the Gene Expression Omnibus data set GSE103876 (Lanver et al. 2018). Gene clustering based on expression profiles was conducted using a hierarchical clustering with an average linkage on a Canberra distance, suitable for expression counts, as implemented in the ‘dist’ and ‘hclust’ functions in R (R Core Team 2018). The resulting clustering tree was converted to a distance matrix and compared to the inferred phylogeny of the genes using a Mantel permutation test, as implemented in the ‘ape’ package for R (Paradis et al. 2004). Differences in expression between time points were assessed by fitting the linear model “expression ~ time * gene”, testing the effect of time while controlling for interaction with the “gene” variable. Residuals were normalized using a Box-Cox transform as implemented in the MASS package for R. Tukey’s posthoc comparisons were conducted on the resulting model, allowing for a 5% false discovery rate.

Acknowledgments

We thank all members of the group for stimulating discussions. We are grateful to Georgiana May and Octavio Paredes-López for providing field isolates of *U. maydis* from the US and Mexico, respectively. We acknowledge the generous support by the Max Planck Society.

References

Altschul SF, Gish W, Miller W, Myers EW, Lipman DJ. 1990. Basic local alignment search tool. *J Mol Biol* **215**: 403–410.

Anisimova M, Gascuel O. 2006. Approximate likelihood-ratio test for branches: A fast, accurate, and powerful alternative. *Syst Biol* **55**: 539–552.

Ast J, Stiebler AC, Freitag J, Bölker M. 2013. Dual targeting of peroxisomal proteins. *Front Physiol* **4**: 297.

Banuett F, Herskowitz I. 1989. Different a alleles of Ustilago maydis are necessary for maintenance of filamentous growth but not for meiosis. *Proc Natl Acad Sci U S A* **86**: 5878–5882.

Barzel A, Obolski U, Gogarten JP, Kupiec M, Hadany L. 2011. Home and away- the evolutionary dynamics of homing endonucleases. *BMC Evol Biol* **11**: 324.

Basse CW. 2010. Mitochondrial inheritance in fungi. *Curr Opin Microbiol* **13**: 712–719.

Belfort M, Roberts RJ. 1997. Homing endonucleases: keeping the house in order. *Nucleic Acids Res* **25**: 3379–3388.

Boidin J. 1986. Intercompatibility and the species concept in the saprobic basidiomycotina. *Mycotaxon* **XXVI**: 319–336.

Charif D, Thioulouse J, Lobry JR, Perrière G. 2005. Online synonymous codon usage analyses with the ade4 and seqinR packages. *Bioinforma Oxf Engl* **21**: 545–547.

Chevalier BS, Stoddard BL. 2001. Homing endonucleases: structural and functional insight into the catalysts of intron/intein mobility. *Nucleic Acids Res* **29**: 3757–3774.

Christianson TW, Sikorski RS, Dante M, Shero JH, Hieter P. 1992. Multifunctional yeast high-copy-number shuttle vectors. *Gene* **110**: 119–122.

Cock PJA, Antao T, Chang JT, Chapman BA, Cox CJ, Dalke A, Friedberg I, Hamelryck T, Kauff F, Wilczynski B, et al. 2009. Biopython: freely available Python tools for computational molecular biology and bioinformatics. *Bioinforma Oxf Engl* **25**: 1422–1423.

Derbyshire V, Kowalski JC, Dansereau JT, Hauer CR, Belfort M. 1997. Two-domain structure of the td intron-encoded endonuclease I-TevI correlates with the two-domain configuration of the homing site. *J Mol Biol* **265**: 494–506.

Djamei A, Kahmann R. 2012. Ustilago maydis: dissecting the molecular interface between pathogen and plant. *PLoS Pathog* **8**: e1002955.

Dong S, Raffaele S, Kamoun S. 2015. The two-speed genomes of filamentous pathogens: waltz with plants. *Curr Opin Genet Dev* **35**: 57–65.

Dujon B, Belfort M, Butow RA, Jacq C, Lemieux C, Perlman PS, Vogt VM. 1989. Mobile introns: definition of terms and recommended nomenclature. *Gene* **82**: 115–118.

Dunin-Horkawicz S, Feder M, Bujnicki JM. 2006. Phylogenomic analysis of the GIY-YIG nuclease superfamily. *BMC Genomics* **7**: 98.

Dutheil JY, Mannhaupt G, Schweizer G, Sieber CMK, Münsterkötter M, Güldener U, Schirawski J, Kahmann R. 2016. A Tale of Genome Compartmentalization: The Evolution of Virulence Clusters in Smut Fungi. *Genome Biol Evol* **8**: 681–704.

Eyre-Walker A, Keightley PD. 2007. The distribution of fitness effects of new mutations. *Nat Rev Genet* **8**: 610–618.

Fischer C. 1957. *Biology and Control of Smut Fungi*. John Wiley & Sons Canada, Limited.

Fuentes I, Karcher D, Bock R. 2012. Experimental reconstruction of the functional transfer of intron-containing plastid genes to the nucleus. *Curr Biol CB* **22**: 763–771.

Gladyshev E. 2017. Repeat-Induced Point Mutation and Other Genome Defense Mechanisms in Fungi. *Microbiol Spectr* **5**.

Goddard MR, Burt A. 1999. Recurrent invasion and extinction of a selfish gene. *Proc Natl Acad Sci U S A* **96**: 13880–13885.

Gogarten JP, Hilario E. 2006. Inteins, introns, and homing endonucleases: recent revelations about the life cycle of parasitic genetic elements. *BMC Evol Biol* **6**: 94.

Gouy M, Guindon S, Gascuel O. 2010. SeaView version 4: A multiplatform graphical user interface for sequence alignment and phylogenetic tree building. *Mol Biol Evol* **27**: 221–224.

Grandaubert J, Lowe RGT, Soyer JL, Schoch CL, Van de Wouw AP, Fudal I, Robbertse B, Lapalu N, Links MG, Ollivier B, et al. 2014. Transposable element-assisted evolution and adaptation to host plant within the Leptosphaeria maculans-Leptosphaeria biglobosa species complex of fungal pathogens. *BMC Genomics* **15**: 891.

Guindon S, Dufayard J-F, Lefort V, Anisimova M, Hordijk W, Gascuel O. 2010. New algorithms and methods to estimate maximum-likelihood phylogenies: assessing the performance of PhyML 3.0. *Syst Biol* **59**: 307–321.

Guy L, Kultima JR, Andersson SGE. 2010. genoPlotR: comparative gene and genome visualization in R. *Bioinforma Oxf Engl* **26**: 2334–2335.

Kaessmann H. 2010. Origins, evolution, and phenotypic impact of new genes. *Genome Res* **20**: 1313–1326.

Kämper J. 2004. A PCR-based system for highly efficient generation of gene replacement mutants in Ustilago maydis. *Mol Genet Genomics MGG* **271**: 103–110.

Kämper J, Kahmann R, Bölker M, Ma L-J, Brefort T, Saville BJ, Banuett F, Kronstad JW, Gold SE, Müller O, et al. 2006. Insights from the genome of the biotrophic fungal plant pathogen Ustilago maydis. *Nature* **444**: 97–101.

Katoh K, Misawa K, Kuma K, Miyata T. 2002. MAFFT: a novel method for rapid multiple sequence alignment based on fast Fourier transform. *Nucleic Acids Res* **30**: 3059–3066.

Khrunyk Y, Münch K, Schipper K, Lupas AN, Kahmann R. 2010. The use of FLP-mediated recombination for the functional analysis of an effector gene family in the biotrophic smut fungus Ustilago maydis. *New Phytol* **187**: 957–968.

Kojic M, Holloman WK. 2012. Brh2 domain function distinguished by differential cellular responses to DNA damage and replication stress. *Mol Microbiol* **83**: 351–361.

Kondrashov FA, Kondrashov AS. 2010. Measurements of spontaneous rates of mutations in the recent past and the near future. *Philos Trans R Soc Lond B Biol Sci* **365**: 1169–1176.

Krombach S, Reissmann S, Kreibich S, Bochen F, Kahmann R. 2018. Virulence function of the Ustilago maydis sterol carrier protein 2. *New Phytol* **220**: 553–566.

Lambowitz AM, Belfort M. 1993. Introns as mobile genetic elements. *Annu Rev Biochem* **62**: 587–622.

Lanver D, Müller AN, Happel P, Schweizer G, Haas FB, Franitza M, Pellegrin C, Reissmann S, Altmüller J, Rensing SA, et al. 2018. The Biotrophic Development of Ustilago maydis Studied by RNA-Seq Analysis. *Plant Cell* **30**: 300–323.

Laurie JD, Ali S, Linning R, Mannhaupt G, Wong P, Güldener U, Münsterkötter M, Moore R, Kahmann R, Bakkeren G, et al. 2012. Genome comparison of barley and maize smut fungi reveals targeted loss of RNA silencing components and species-specific presence of transposable elements. *Plant Cell* **24**: 1733–1745.

Le SQ, Gascuel O. 2008. An improved general amino acid replacement matrix. *Mol Biol Evol* **25**: 1307–1320.

Lloyd AH, Timmis JN. 2011. The origin and characterization of new nuclear genes originating from a cytoplasmic organellar genome. *Mol Biol Evol* **28**: 2019–2028.

Louis EJ, Haber JE. 1991. Evolutionarily recent transfer of a group I mitochondrial intron to telomere regions in Saccharomyces cerevisiae. *Curr Genet* **20**: 411–415.

Lynch M. 2007. *The Origins of Genome Architecture*. Sinauer Associates.

Lynch M, Sung W, Morris K, Coffey N, Landry CR, Dopman EB, Dickinson WJ, Okamoto K, Kulkarni S, Hartl DL, et al. 2008. A genome-wide view of the spectrum of spontaneous mutations in yeast. *Proc Natl Acad Sci U S A* **105**: 9272–9277.

Mewes HW, Ruepp A, Theis F, Rattei T, Walter M, Frishman D, Suhre K, Spannagl M, Mayer KFX, Stümpflen V, et al. 2011. MIPS: curated databases and comprehensive secondary data resources in 2010. *Nucleic Acids Res* **39**: D220-224.

Möller M, Stukenbrock EH. 2017. Evolution and genome architecture in fungal plant pathogens. *Nat Rev Microbiol* **15**: 756–771.

Ohta T. 2000. Evolution of gene families. *Gene* **259**: 45–52.

Paradis E, Claude J, Strimmer K. 2004. APE: Analyses of Phylogenetics and Evolution in R language. *Bioinforma Oxf Engl* **20**: 289–290.

Perrière G, Thioulouse J. 2002. Use and misuse of correspondence analysis in codon usage studies. *Nucleic Acids Res* **30**: 4548–4555.

R Core Team. 2018. *R: A Language and Environment for Statistical Computing*. R Foundation for Statistical Computing https://www.R-project.org/.

Ranwez V, Harispe S, Delsuc F, Douzery EJP. 2011. MACSE: Multiple Alignment of Coding SEquences accounting for frameshifts and stop codons. *PloS One* **6**: e22594.

Sánchez-Alonso P, Guzmán P. 1998. Organization of chromosome ends in Ustilago maydis. RecQ-like helicase motifs at telomeric regions. *Genetics* **148**: 1043–1054.

Schirawski J, Mannhaupt G, Münch K, Brefort T, Schipper K, Doehlemann G, Di Stasio M, Rössel N, Mendoza-Mendoza A, Pester D, et al. 2010. Pathogenicity determinants in smut fungi revealed by genome comparison. *Science* **330**: 1546–1548.

Schweizer G, Münch K, Mannhaupt G, Schirawski J, Kahmann R, Dutheil JY. 2018. Positively Selected Effector Genes and Their Contribution to Virulence in the Smut Fungus Sporisorium reilianum. *Genome Biol Evol* **10**: 629–645.

Singh DK, Ghosh AK, Croteau DL, Bohr VA. 2012. RecQ helicases in DNA double strand break repair and telomere maintenance. *Mutat Res* **736**: 15–24.

Steinberg G, Perez-Martin J. 2008. Ustilago maydis, a new fungal model system for cell biology. *Trends Cell Biol* **18**: 61–67.

Stoddard BL. 2005. Homing endonuclease structure and function. *Q Rev Biophys* **38**: 49–95.

Sun CW, Callis J. 1993. Recent stable insertion of mitochondrial DNA into an Arabidopsis polyubiquitin gene by nonhomologous recombination. *Plant Cell* **5**: 97–107.

Thorsness PE, Weber ER. 1996. Escape and migration of nucleic acids between chloroplasts, mitochondria, and the nucleus. *Int Rev Cytol* **165**: 207–234.

Valverde ME, Vandemark GJ, Martínez O, Paredes-López O. 2000. Genetic diversity of Ustilago maydis strains. *World J Microbiol Biotechnol* **16**: 49–55.

Volff J-N. 2006. Turning junk into gold: domestication of transposable elements and the creation of new genes in eukaryotes. *BioEssays News Rev Mol Cell Dev Biol* **28**: 913–922.

Vollmeister E, Schipper K, Baumann S, Haag C, Pohlmann T, Stock J, Feldbrügge M. 2012. Fungal development of the plant pathogen Ustilago maydis. *FEMS Microbiol Rev* **36**: 59–77.

Tables

Table 1: *UMAG_11065* paralogs in *U. maydis*, together with a homolog from *F. oxysporum* for comparison.

Gene	Chr / Scaffold / Contig	Start	End	Length of Chr / Scaffold / Contig	Number of introns	Length of protein	Relative position (1)
UMAG_06476	Chromosome 3	1641500	1642057	1642070	0	185	99.98%
UMAG_06474	Chromosome 3	1639598	1640203	1642070	0	201	99.87%
UMAG_06506	Chromosome 7	951043	954234	957188	5	983	99.52%
UMAG_10585	Chromosome 4	883585	884046	884984	0	153	99.87%
UMAG_11065	Chromosome 9	1886	1263	733962	0	207	0.21%
UMAG_03394	Chromosome 9	8836	5960	733962	0	958	1.01%
UMAG_03869	Chromosome 10	687301	690648	692354	7	937	99.51%
UMAG_04094	Chromosome 11	688670	689965	690620	0	431	99.81%
UMAG_04486	Chromosome 14	605233	609089	611467	2	1175	99.30%
UMAG_04308	Chromosome 14	1241	87	611467	0	384	0.11%
UMAG_05977	Chromosome 20	523510	523884	523884	0	124	99.96% (2)
UMAG_10980	Chromosome 22	398220	400499	403590	0	759	98.95%
UMAG_12076	Contig 1.265	4214	5343	5343	0	376	89.43%
FOXG_04692	Supercontig 2.5	9736	6398	2688632	0	1112	0.30%

(1) Position reported to the length of the chromosome or contig.

(2) N-terminal fragment only.

Table 2: Detection of the *UMAG_11064,* and *UMAG_11072* genes in several *U. maydis* and *S. reilianum* strains.

Region	Strain											
	U. maydis									*S. reilianum*		
	SG200	10-1	518	521	I2	O2	P2	S5	T6	JS161	SRZ1	SRZ2
UMAG_11064 ORF	+	-	+	+	-	-	-	-	-	+	+	+
UMAG_11072 ORF	+	+	+	+	+	+	+	+	+			
Cox1 Exon 1+2	254	254	254	254	254	254	254	254	254	1607	1607	1607
Cox1 Exon 7	1306	1306	1306	1306	1306	1306	1306	1306	1306	161	161	161

Plus and minus signs indicate whether the corresponding gene could be amplified or not. Numbers indicate the size of the amplified region in base pairs.

Supplementary Table S1: Homology search results using *UMAG_11064* as a query on the NCBI non-redundant nucleotide database, using BlastN. All hits with an E-value lower than 1E-04 are included, alongside with corresponding alignment length and percentage of sequence identity.

Supplementary Table S2: Homology search results using *UMAG_11064* as a query on NCBI non-redundant protein database, using BlastP. All hits with an E-value lower than 1E-04 are included, alongside with corresponding alignment length and percentage of sequence identity.

Supplementary Table S3: Homology search results using *UMAG_11065* as a query on NCBI non-redundant protein database, using BlastP. All hits with an E-value lower than 1E-04 are included, alongside with corresponding alignment length and percentage of sequence identity.

Supplementary Table S4: Homology search results using *U. maydis cox1* intron 6 as a query on a NCBI non-redundant protein database, using BlastX. All hits with an E-value lower than 1E-04 are included, alongside with corresponding alignment length and percentage of sequence identity.

Supplementary Table S5: Homology search results using *S. reilianum cox1* intron 1 as a query on a NCBI non-redundant protein database, using BlastX. All hits with an E-value lower than 1E-04 are included, alongside with corresponding alignment length and percentage of sequence identity.

Supplementary Table S6: Homology search results using *S. reilianum cox1* intron 2 as a query on a NCBI non-redundant protein database, using BlastX. All hits with an E-value lower than 1E-04 are included, alongside with corresponding alignment length and percentage of sequence identity.

Supplementary Table S7: Primers used in this study.

Figures

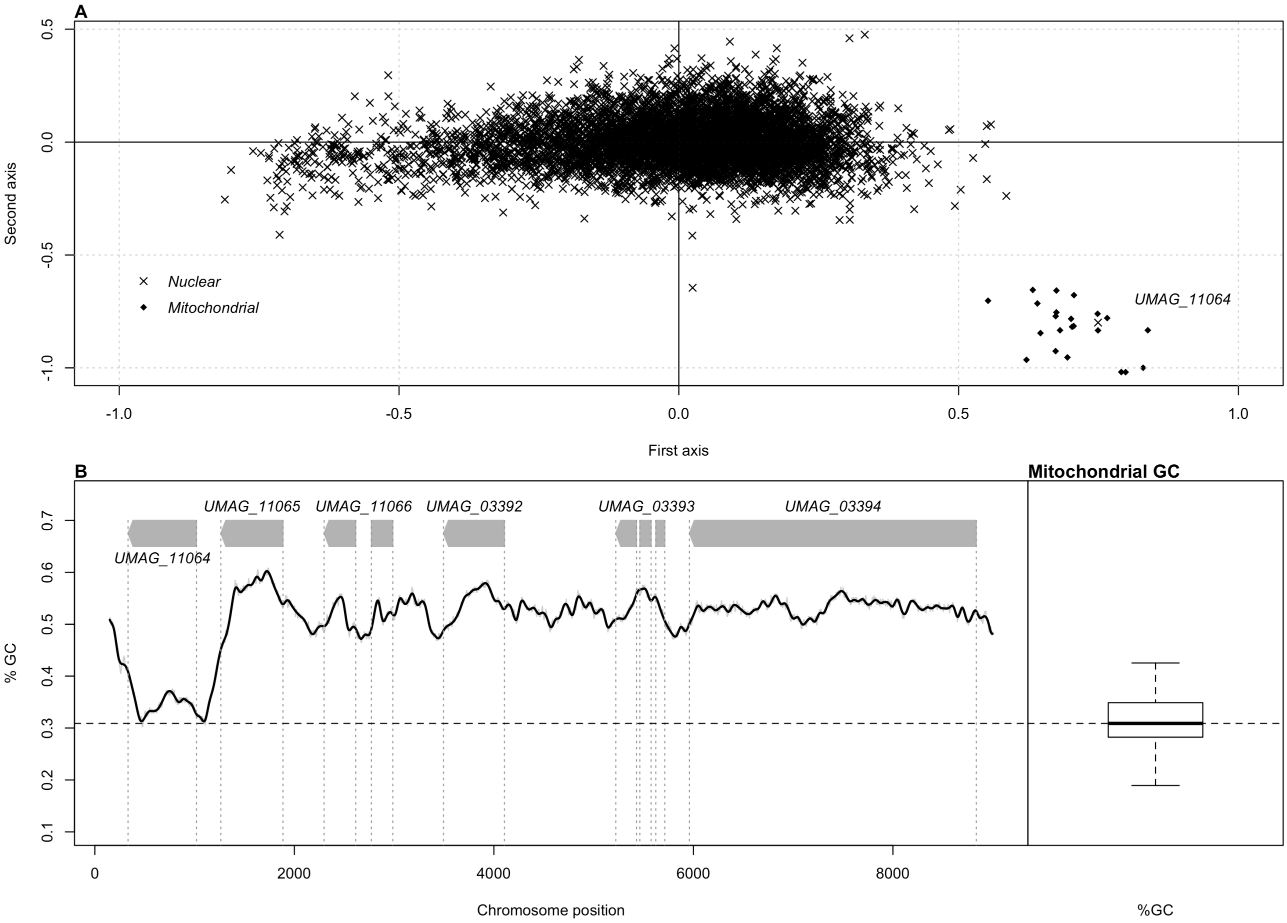

Figure 1: Identification of the *UMAG_11064* gene. A) Codon usage analysis in *U. maydis*. B) Genomic context of the gene *UMAG_11064*. GC content in 300 bp windows sliding by 1 bp, and distribution of GC content in 300 bp windows of mitochondrial genome of *U. maydis*. The dash line represents the median of the distribution.

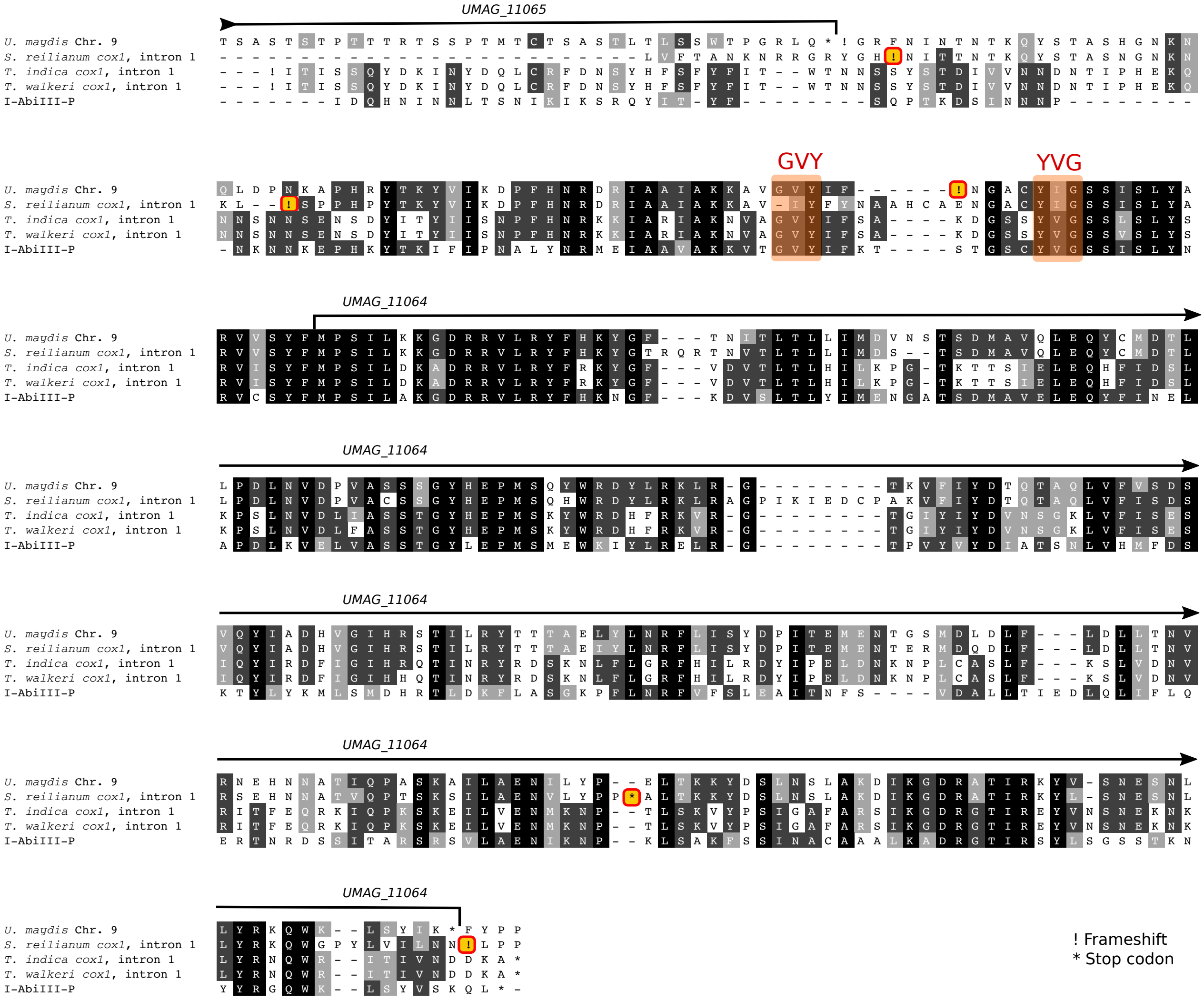

Figure 2: Alignment of *UMAG_11064* and its upstream sequence with intron 1 from the *cox1* gene of *S. reilianum*, *T. indica* and *T. walkeri*, as well as the coding sequence of the *A. bisporus* HE. Shading indicates the level of amino-acid conservation. Amino-acids noted as 'X' have incomplete codons due to frameshifts. Highlighted exclamation marks denote inferred frameshifts and '*' characters stop codons. The location of the active site of the HE (GVY-YVG) is highlighted.

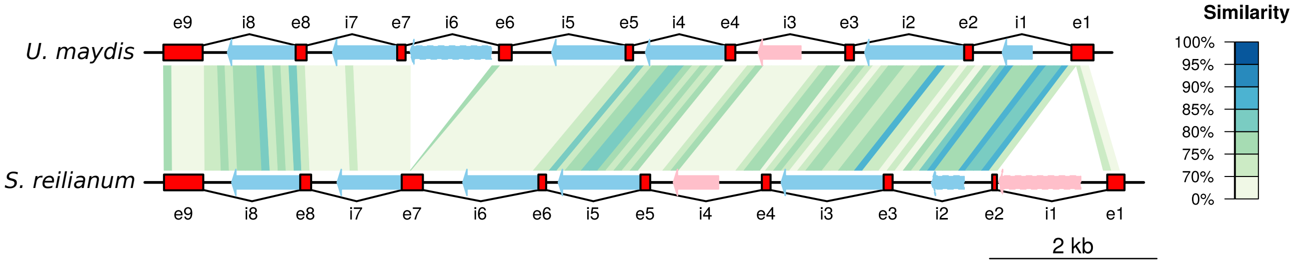

Figure 3: Intron structure of the *cox1* gene in *U. maydis* and *S. reilianum*. Annotated HEs are indicated. Red boxes depict *cox1* exons, numbered from *e1* to *e9*. Introns are represented by connecting lines and numbered *i1* to *i8*. Arrows within introns show LAGLIDADG (light blue) and GIY-YIG HEs (pink). Dashed arrows correspond to HEGs inferred by blast search, while solid arrows correspond to the annotation from the GenBank files. Piecewise sequence similarity between *U. maydis* and *S. reilianum* is displayed with a color gradient.

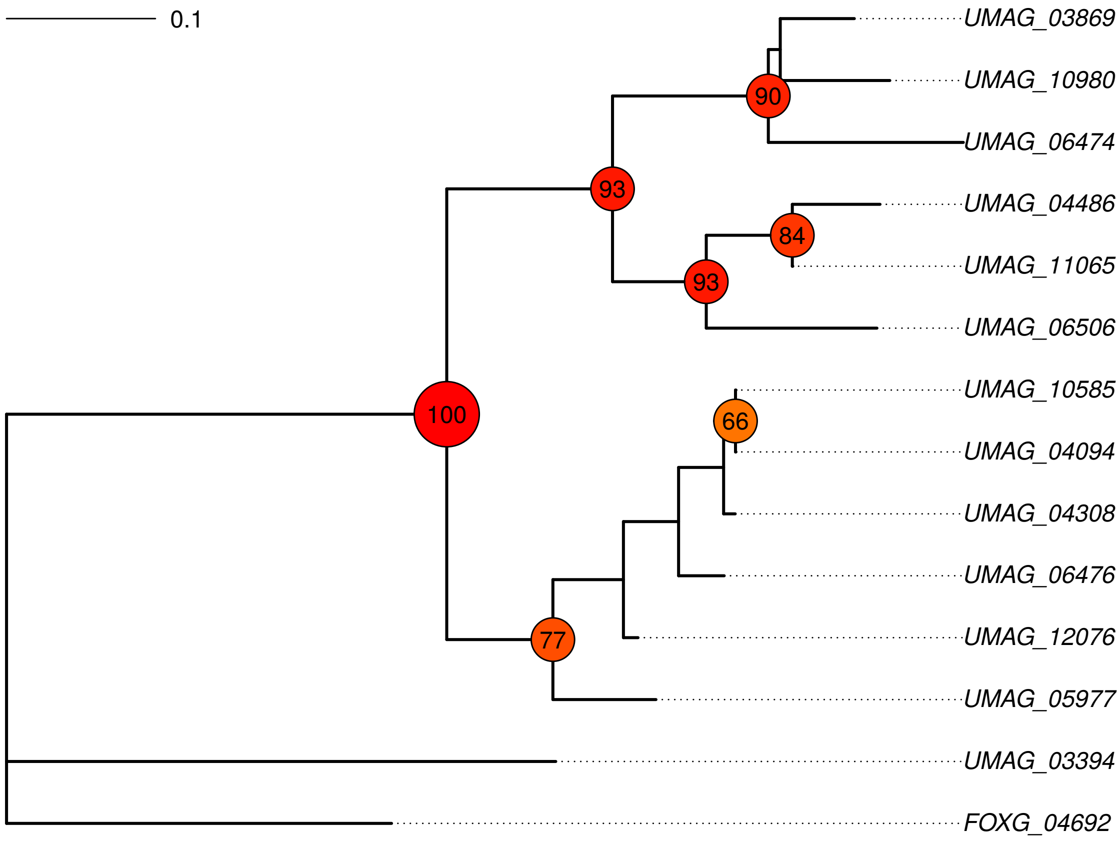

476 **Figure 4:** Maximum likelihood phylogeny of *UMAG_11065 U. maydis* paralogs together with the closest homolog from *F. oxysporum* (see Table 1). Support values higher than 0.6 are reported.

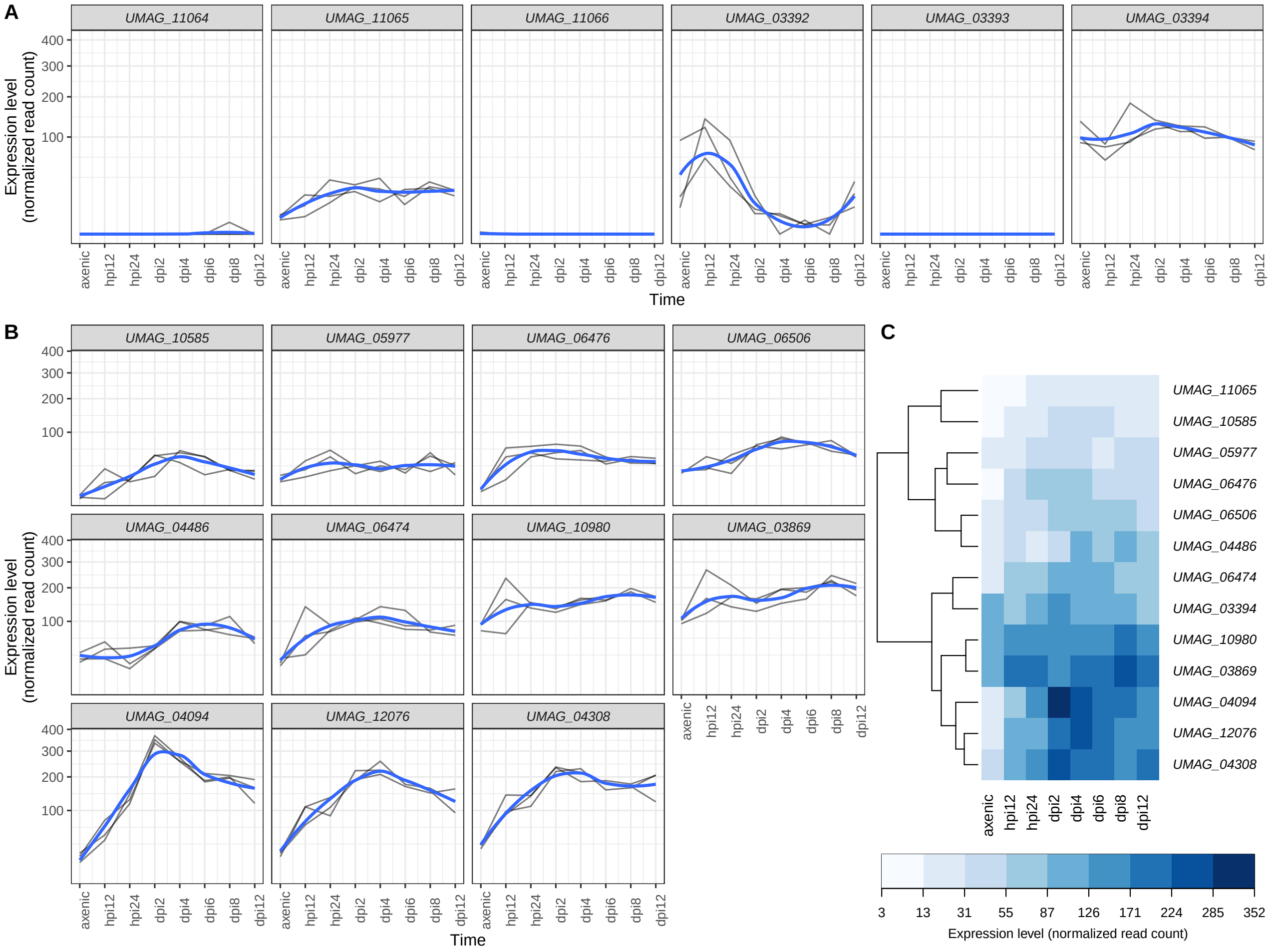

481 **Figure 5:** Patterns of gene expression for *UMAG_11064* and *UMAG_11065*, together with neighboring and homologous genes. A) Gene expression profiles for genes in the chromosome 9 telomeric region (as depicted on Figure 1B). Straight lines represent three independent replicates, while the blue curve depicts the smoothed conditional mean computed using the LOESS method. B) Gene expression profiles for the *UMAG_11065* homologs (Figure 4). Legends as in A. C) Clustering of the *UMAG_11065* homologs based on their averaged expression profile (see Methods). Hpi: hours post-infection. Dpi: days post-infection.

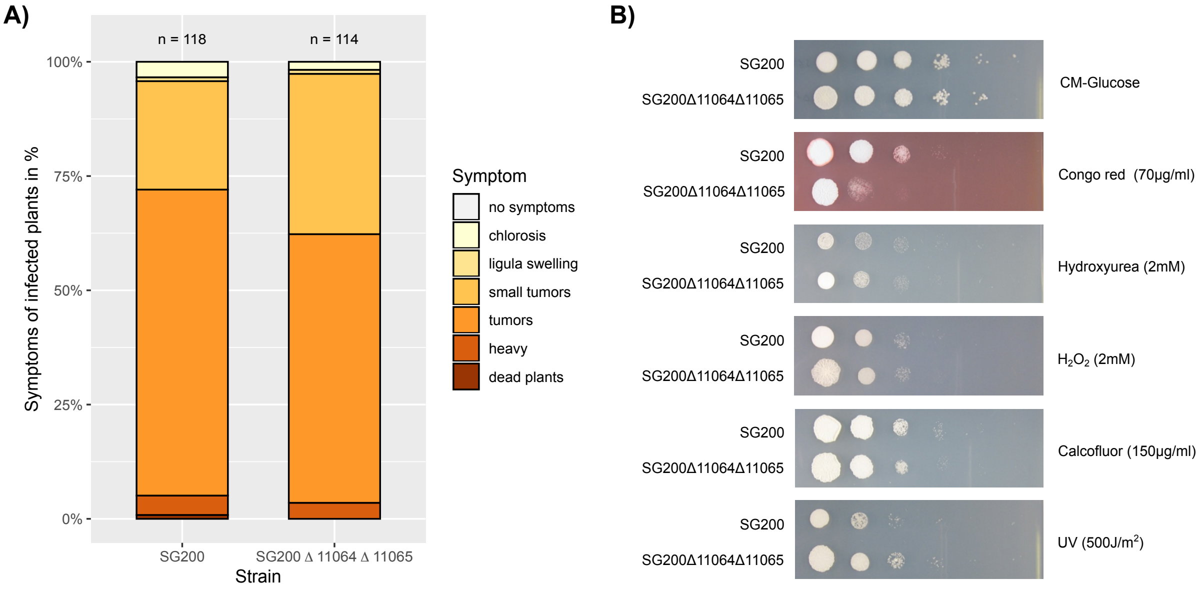

Figure 6: Phenotype assessment of the double deletion strain. A) The simultaneous deletion of *UMAG_11064* and *UMAG_11065* does not affect virulence. Maize seedlings were infected with the indicated strains. Disease symptoms were scored at 12 dpi according to Kämper et al. (Kämper et al. 2006) using the color code depicted on the right. Colors reflect the degree of severity, from brown-red (severe) to light yellow (mild). Data represent mean of n = 3 biologically independent experiments. Total numbers of infected plants are indicated above the respective columns. B) Stress assay of the double deletion strain (Δ11064Δ11065), lacking both genes *UMAG_11064* and *UMAG_11065*, compared to the parental SG200 strain.

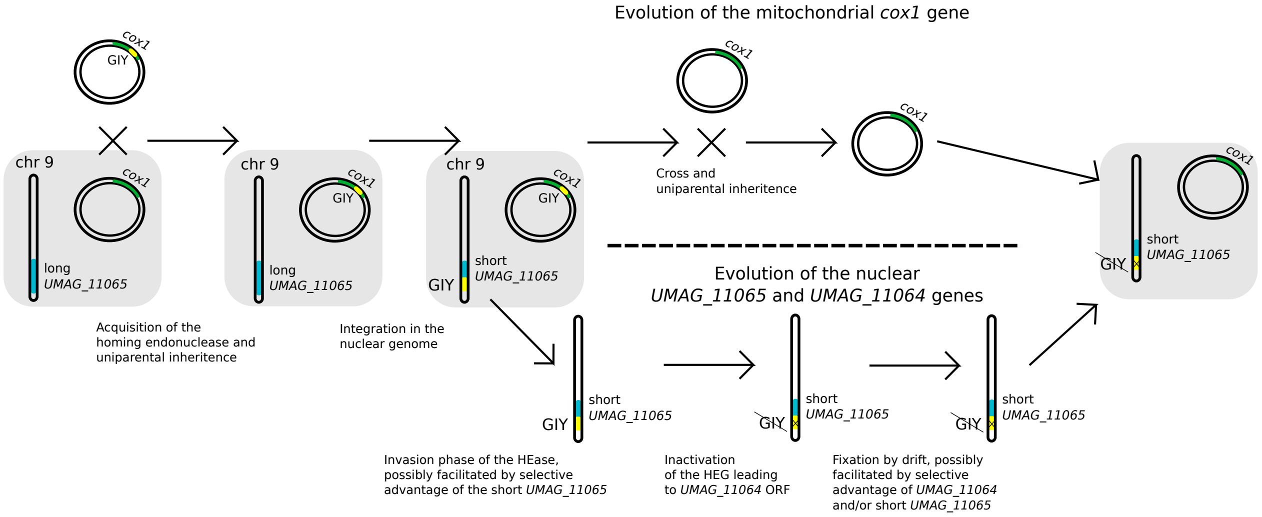
Evolution of the mitochondrial *cox1* gene
cox1
GIY
chr 9
long
UMAG_11065
short
UMAG_11065
Acquisition of the homing endonuclease and uniparental inheritence
Integration in the nuclear genome
Cross and uniparental inheritence
Evolution of the nuclear *UMAG_11065* and *UMAG_11064* genes
Invasion phase of the HEase, possibly facilitated by selective advantage of the short *UMAG_11065*
Inactivation of the HEG leading to *UMAG_11064* ORF
Fixation by drift, possibly facilitated by selective advantage of *UMAG_11064* and/or short *UMAG_11065*

Figure 7: Possible evolutionary scenario recapitulating the events leading to the formation of the *UMAG_11064* and *UMAG_11065 U. maydis* genes.

Supplementary Figure S1: Amplification of the candidate region in the telomeric region of chromosome 9. A) Genomic context based on the *U. maydis* reference genome, and location PCR primers. B) PCR results with corresponding expected fragment sizes. Primer sequences are provided in Table S7.

Supplementary Figure S2: Amplification of *UMAG_11064*, *UMAG_11072* and *cox1* exons 1 and 7 in several *U. maydis* and *S. reilianum* strains. Strains are as in Table 2. Primer sequences are provided in Table S7.

Supplementary Figure S3: Verification of the deletion of *UMAG_11064* and *UMAG_11065*. A) Schematic map of the genomic region containing *UMAG_11064* and *UMAG_11065* in SG200 and SG200Δ11064Δ11065. Primers used to amplify the left and right border sequences are indicated. B) DNA of SG200 and SG200Δ11064Δ11065 was cleaved with Fsp1 and subjected tho southern blot analysis using a mixture of Probes 1 and 2 indicated in A). The 2.94 kb fragment is diagnostic for SG200 while the 4.19 kb fragment is diagnostic for the deletion of *UMAG_11064* and *UMAG_11065.*

Supplementary file:

Supplementary File S1: Scripts used to conduct the phylogenetic and statistical analyses, As well as R code used to generate figures 1, 3, 4, 5 and 6.